Novel Gadolinium-Free Ultrasmall Nanostructured Positive Contrast for Magnetic Resonance Angiography and Imaging

Rodrigo Ken Kawassaki[1], Mariana Romano[1], Mayara Klimuk Uchiyama[1,2], Roberta Mansini Cardoso[1], Maurício da Silva Baptista[3], Sandra Helena Poliselli Farsky[4], Khallil Taverna Chaim[2,5], Robson Raphael Guimarães[1], Koiti Araki[1,*]

[1] Laboratory of Supramolecular Chemistry and Nanotechnology, Department of Fundamental Chemistry, Institute of Chemistry, University of São Paulo, São Paulo, Brazil

[2] Laboratory of Magnetic Resonance in Neuroradiology (LIM44), School of Medicine, University of São Paulo, São Paulo, Brazil

[3] Laboratory of Interfaces and Photoinduced Processes, Department of Biochemistry, Institute of Chemistry, University of São Paulo, São Paulo, Brazil

[4] Laboratory of Inflammation and Immunotoxicology, Department of Clinical and Toxicological Analysis, Faculty of Pharmaceutical Sciences, University of São Paulo, São Paulo, Brazil

[5] Imaging Platform (PISA), Hospital das Clínicas HCFMUSP, School of Medicine, University of São Paulo, São Paulo, Brazil

(*) Koiti Araki

E-mail: koiaraki@iq.usp.br

ABSTRACT

Nanostructured contrast agents are promising alternatives to Gd(III)-based chelates in magnetic resonance (MR) imaging techniques. A novel ultrasmall paramagnetic nanoparticle (UPN) was strategically designed to maximize the number of exposed paramagnetic sites and r_1 while minimizing r_2, by decorating 3 nm large titanium dioxide nanoparticles with suitable amounts of iron oxide. Its relaxometric parameters are comparable to that of gadoteric acid (GA) in agar phantoms, and the r_2/r_1 ratio of 1.38 at 3T is close to the ideal unitary value. The good contrast effect was confirmed by T1-weighted MR images of Wistar rats after intravenous bolus injection of UPN. Those results associated with good biocompatibility and a much longer contrast effect before renal excretion indicate its high potential as alternative blood-pool contrast agent to the GA gold standard for MR angiography, especially for patients with severe renal impairment.

KEY-WORDS: *Ultrasmall Nanoparticle, Paramagnetic, Contrast Agent, MRI, Iron Oxide*

Magnetic resonance imaging (MRI) is a noninvasive diagnosis technique that provide detailed anatomic information of soft tissues whose image resolution to detect injuries is further improved by contrast agents (CAs). Their effect is based on the shortening of the longitudinal (spin-lattice, T_1) and transverse (spin-spin, T_2) relaxation times, and can be classified as T_1-/positive or T_2-/negative CAs depending on the contrast efficiency measured by their longitudinal (r_1) and transverse (r_2) relaxivities. The overall relaxation time is given by the sum of both phenomena but tend to be more strongly associated with the dephasing rate in the *xy* plane than the decay to the magnetic ground state. Hence, the positive CAs are those presenting a r_2/r_1 ratio closer to 1, the ideal value, whereas negative CAs typically exhibit ratios larger than about 5.[1,2]

The current FDA-approved CAs are based on Gd^{3+}or Mn^{2+} chelates, and iron oxide nanoparticles (IONPs).[3–5] In the 1980s, Gd^{3+} was evaluated as the most effective paramagnetic ion for T_1-weighted images[3], thus making it the most preferred in clinical practices for increasing the brightness of blood vessels and surrounding tissues in the MR images. It is administered as chelated compounds, and recently as more stable macrocyclic compounds, to avoid adverse effects of toxic free Gd^{3+} ion. However, recent studies associated the development of nephrogenic systemic fibrosis to such Gd^{3+}-based contrast agents (GBCAs), especially in patients with renal impairment.[6–8] Furthermore, repeated

exposure to GBCAs can lead to deposition of Gd^{3+} in organs such as bones, skin, kidneys and even in the brain, igniting a warning alert on the possible associated threats.[7–9]

Nanomaterials have been studied as more versatile and promising alternatives since their properties can be modulated by controlling their physico-chemical characteristics[10,11]. Three are the main types: 1) those whose core material (Fe_2O_3, Gd_2O_3, MnO) is paramagnetic;[12–14] 2) those doped with paramagnetic ions;[15,16] and 3) those conjugated/coordinated to paramagnetic ions such as Gd^{3+}, Dy^{3+}, Fe^{3+}, Mn^{2+}.[17–19] Among these, the most explored as potential nanocontrast agents are the superparamagnetic iron oxide nanoparticles (SPIONs), due to their high biodegradability and non-toxicity in biological systems when compared to GBCAs.[20–24] However, despite their much larger intrinsic magnetic moments, those materials still are behind conventional GBCAs and deliver inferior contrast performance. SPIONs have high r_2/r_1 values (typically above 10) which imply in hyposignal (darkening of the surrounding region) in T_2-weighted images in routine MRI which may be mistaken with other hypointense areas caused by bleeding, calcification, and metal deposits, as well as the blooming effect.[1,2]

The recent development of CAs based on ultrasmall IONPs (USIONs < 5 nm) brought a significant improvement since they can behave as T_1-CAs.[25–29] It was shown that their r_1 and r_2/r_1 ratio are strongly dependent on nanoparticles size, shape and core crystallinity, as well as surface interactions and aggregation state in the biological environment.[1,2,30,31] Therefore, USIONs with relevant parameters approaching the ideal ones, especially lower r_2/r_1 ratios, have been reported.[1] Yet, the translation to clinical use is still a challenge as other issues also need to be overcome, such as scaling up process improving production cost, colloidal stability, application protocol and pharmacological parameters. Interestingly, Ferumoxytol, an USION-based formulation registered for treatment of anemia administered by slow infusion, is being explored as off-label alternative to GBCAs.[32] Hence, many efforts are underway in the quest of safer CAs, but no alternative product to GBCAs with comparable clinical performance and similar clinical practice protocol has been consolidated in the market yet.

Accordingly, herein is presented a novel class of ultrasmall paramagnetic nanoparticles (UPNs) with adjustable magnetic and MRI-contrast properties by decorating biocompatible ultrasmall titanium dioxide nanoparticles (usTiO_2NPs) with suitable amounts of iron oxide. The properties of such novel engineered nanomaterials were carefully adjusted to overcome the key issues faced by GBCAs and SPION-based products, including no toxic elements and no significant toxicity, thus avoiding nephrotoxicity and metal accumulation.

The safety issues were further assessed by carrying out careful systematic stability studies in biological medium and toxicological assays based on cell viability tests. In addition, r_2/r_1 values was adjusted to be lower than 2 to overcome the limitation of SPIONs as typical T_2-CAs, thus enabling T_1-contrast images with quality as high as using GBCAs as demonstrated *in vivo*. In addition, UPNs are fully compatible with the currently used clinical imaging protocols while providing extended vascular contrast for a period up to 20 minutes, which can be convenient in most cases.

The NPs were produced by non-hydrolytic method and stabilized with selected functionalizing ligands. The size and morphology were determined by dynamic light scattering (DLS) and transmission electron microscopy (TEM) images, complementary techniques that provide information in aqueous dispersion and in the solid state, respectively. TEM image revealed monodisperse and non-agglomerated spherical UPNs with an average core size of 3 nm (dark spots, **Figure 1a**). Its high dispersibility in water was confirmed by DLS that provided an average size of 3.8 nm (**Figure 1b**) with no additional peak in the volume-weighted histograms, as expected for monodisperse NPs. The slightly larger diameter by DLS is expected since it measures the hydrodynamic diameter which includes the functionalizing molecular layer and the hydration layer. Finally, given the very small size and high concentration of surface defects, the NPs must exhibit low crystallinity, as demonstrated by a X-ray diffractogram (XRD) showing only a broad halo characteristic of amorphous materials around 20º 2θ (**Figure 1c**), revealing unexpectedly higher structural disorder. This can be better evaluated by comparison with the XRD pattern of SPIONs, that typically exhibits characteristic diffraction peaks.[33]

Moreover, nanomaterials intended to biomedical applications need to be colloidally stable in biological systems, but NPs tend to agglomerate/aggregate, as the ionic strength increases, or when in the presence of other substances.[34] Accordingly, their colloidal stability in biological media, such as cell culture media, need to be evaluated since aggregated nanoparticles often show negative biological responses (inflammation, ROS, loss of functionality),[35–38] and also can induce the coupling of their magnetic moments influencing the r_2/r_1 ratio value.[31,39,40] Hence, the size distribution of the UPN functionalized with different ligands (citrate (Cit), glycerol-3-phosphate (Gly), *o*-phosphorylethanolamine (PEA) or tiron (Tir)) (0.25 mM Fe) in RPMI-1640 cell culture medium supplemented with fetal bovine serum (FBS) 10% (v/v) was monitored by DLS. The volume-weighted histogram showed no change after 24h and 48h of incubation **(Figure 1d**) indicating no aggregation.

When administered by intravenous (i.v.) injection, NPs will interact with all blood components (biomolecules, salts, circulating blood cells) and vessel walls (endothelial cells). Their permanence in circulation will depend on these interactions and the clearance systems of the body, such as the mononuclear phagocyte system. The blood clearance can be performed by specialized cells such as tissue macrophages, especially if their size is > 5.5 nm.[41–43] Hence, the *in vitro* toxicity of UPNs functionalized with the same ligands series was assessed by the MTT and resazurin methods using HUVEC and RAW 264.7 cell lines as relevant models of endothelial cells and macrophages, respectively, by comparing the cell viability after 24h of exposure to UPN (0.25 mM Fe) with controls (culture medium). There was no significative reduction on HUVEC cells viability treated with UPN as compared with controls ($p < 0.05$) (**Figure 1e**). In contrast, the treatment with UPNs caused a small reduction on the RAW 264.7 cells viability **(Figure 1f)** in comparison with control in both, MTT and resazurin assays ($p > 0.05$), but the cell viability remained above 70% in both cases, and could not be considered potentially cytotoxic.[44]

The volume- and intensity-weighted size distribution histograms were compared to make clear the DLS pattern associated with UPNs (**Figures 1d** and **1Sa**, respectively) and proteins present in the culture medium supplemented with FBS (**Figure 1Sc**).[45,46] Since UPNs and proteins have similar sizes (3 and 10 nm), it is reasonable evaluating the size distribution by volume and by intensity rather than by number to assess the colloidal stability and the eventual formation of a biomolecular corona. Interestingly, the NPs seems to be found in two states, a dissociated one (~10 nm) and a much larger associated state (~100 nm) (**Figure 1Sa**). The shift of the peak from about 10 nm (time zero) to 100 nm after 24 and 48h with a contrasting size distribution pattern relative to control (**Figure 1Sa**), clearly indicates the UPNs interaction with protein particles favoring the associated state, which can be related to a corona layer but not to aggregation.[45,47] Such process is reproducible and seems to be controlled by specific NPs/protein interactions, given their similar negative zeta potentials (ZPs) (**Figure 1Sd**). The similar size distribution patterns (**Figure 1Sa**) with absence of further precipitation (**Figure 1Sb**) indicates they are suitable for biological application.

The UPNs functionalized with different ligands presented negative ZPs, with the citrate derivative presenting the lowest ZP. Thus, a formulation with 25 mM of Fe and 150 mM of propylene glycerol, to adjust the osmolarity to 1600 mOsm/kg H_2O, was prepared, filtered through 0.22 µm filter and sealed in 2 mL sterile amber glass ampoules, in good practice conditions, for use in the biological assays. The formulated UPNs has a ZP of -34.7 ± 5.5 mV and formed a nanofluid containing individually dispersed nanoparticles.

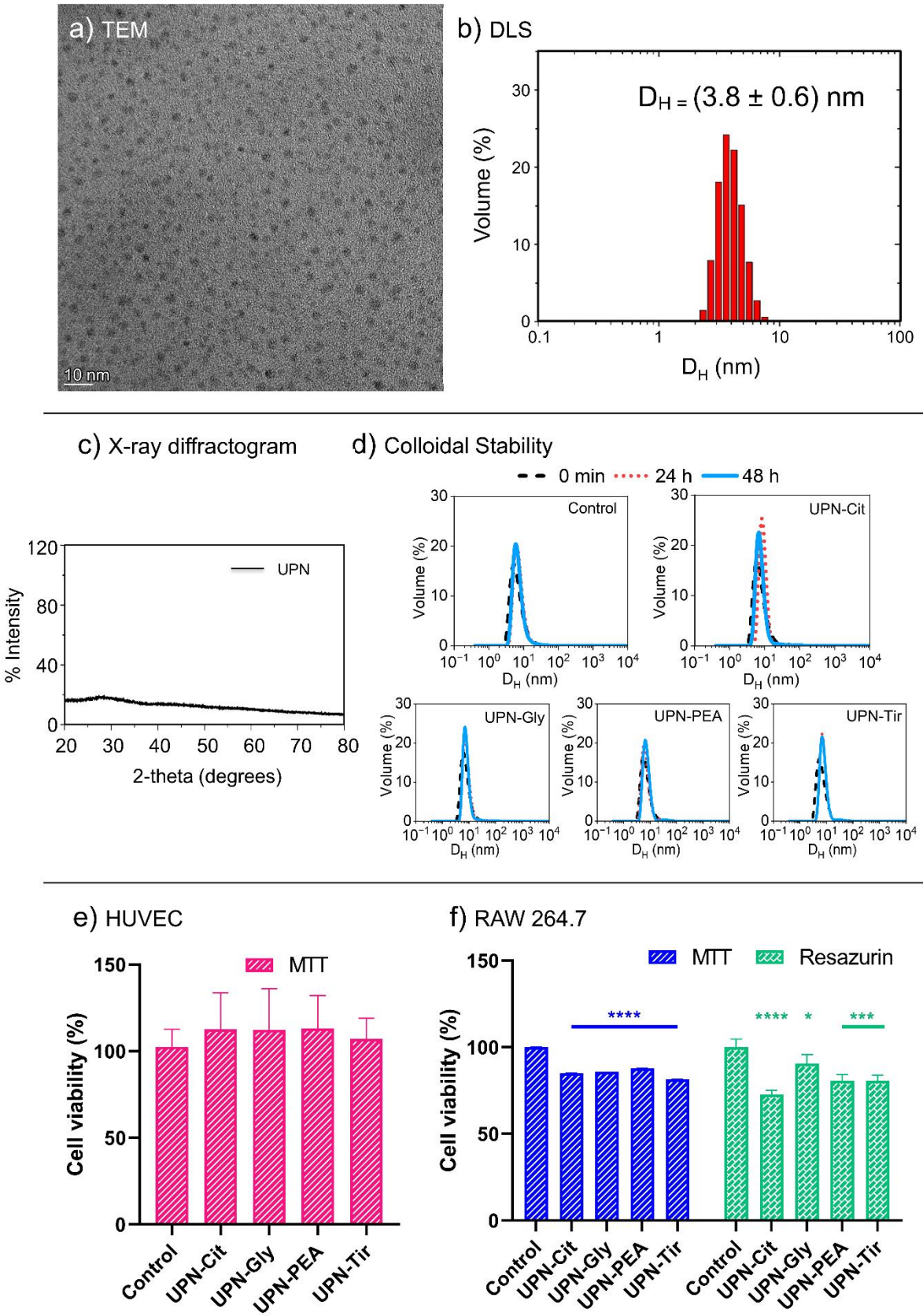

Figure 1. Characterization and *in vitro* toxicity studies of UPN: (a) TEM image showing the well-dispersed nanoparticles, (b) hydrodynamic size distribution histogram by volume-weighted DLS, and

(c) X-ray diffractogram of the UPN showing the amorphous structure. (d) UPNs colloidal stability in RPMI-1640 cell culture medium supplemented with FBS 10% (v/v) evaluated by DLS (volume-weighted size distribution) after 0 min, 24h and 48h of incubation. MTT and resazurin cytotoxicity assay of UPNs (0.25 mM Fe) functionalized with citrate (Cit), glycerol-3-phosphate (Gly), *o*-phosphorylethanolamine (PEA) and tiron (Tir) against (e) HUVEC and (f) RAW 264.7 cell lines after 24h of incubation. ANOVA: * $p < 0.05$; *** $p < 0.0005$; **** $p < 0.0001$.

The transversal spin relaxivity and magnetization are two related key parameters that are sensitive to the size and degree of crystallinity of SPIONs, that are typical T_2-CAs since their much higher magnetization is very effective in generating more extended magnetic inhomogeneities responsible for spin-spin relaxation processes (high r_2 and r_2/r_1 values). In contrast, the longitudinal spin relaxivity responsible for the T_1-contrast, is strongly dependent on the direct interaction of the water molecules with the CAs paramagnetic sites.[1] Thus, GBCAs have a labile coordination site for interaction with water molecules to optimize r_1.[7] This implies that smaller nanoparticles with larger surface areas tend to be better suited as alternatives since increasingly larger amounts of the paramagnetic ion will be exposed at the surface promoting the spin-lattice relaxation.[1] Additionally, paramagnetic ions in nanoparticles induce the lowest as possible disturbance on the local magnetic field (lower r_2) due to surface spin-canting effect.[1,2] This reduces their saturation magnetization since the magnetically dead surface volume relative to its inner core tend to increase as the size decreases.[26] Hence, the sum of effects leads to a higher r_1, while r_2 decreases and the r_2/r_1 ratio tends to 1. Shen *et al.* (2017) found that 3.6 nm diameter poly(acrylic acid) stabilized IONPs presented low r_2/r_1 ratio (2.6 at 1.5T, and 10.5 at 7T),[27] whereas Kim *et al*. (2011) showed that 1.5 nm large IONPs exhibit a magnetization behavior similar to paramagnetic materials.[26] The herein described UPNs are usTiO_2NPs decorated with paramagnetic iron oxide that fulfills the requirements for application as MRI CAs.

The gadoteric acid (GA) is the gold standard T_1-CAs in clinical MRI diagnostics, hence its MR relaxometric properties were compared with that of the novel UPNs in agar phantoms. Its r_1 and r_2 were determined to be 1.76 mM^{-1} s^{-1} and 2.43 mM^{-1} s^{-1} at 3T, and 1.32 mM^{-1} s^{-1} and 2.35 mM^{-1} s^{-1} at 7T, as compared to 7.32 mM^{-1} s^{-1} and 4.84 mM^{-1} s^{-1} at 3T and 3.80 mM^{-1} s^{-1} and 3.53 mM^{-1} s^{-1} at 7T of GA (**Figure 2a** and **2b**). Thus, the r_2/r_1 ratio for the UPN is 1.38 (3T) and 1.78 (7T), in comparison with 0.66 (3T) and 0.93 (7T) for GA, typical parameters of T_1-contrast agents. Interestingly, the relaxivity of UPN is much less sensitive to the magnetic field than GA, being promising as CAs in high field equipments.

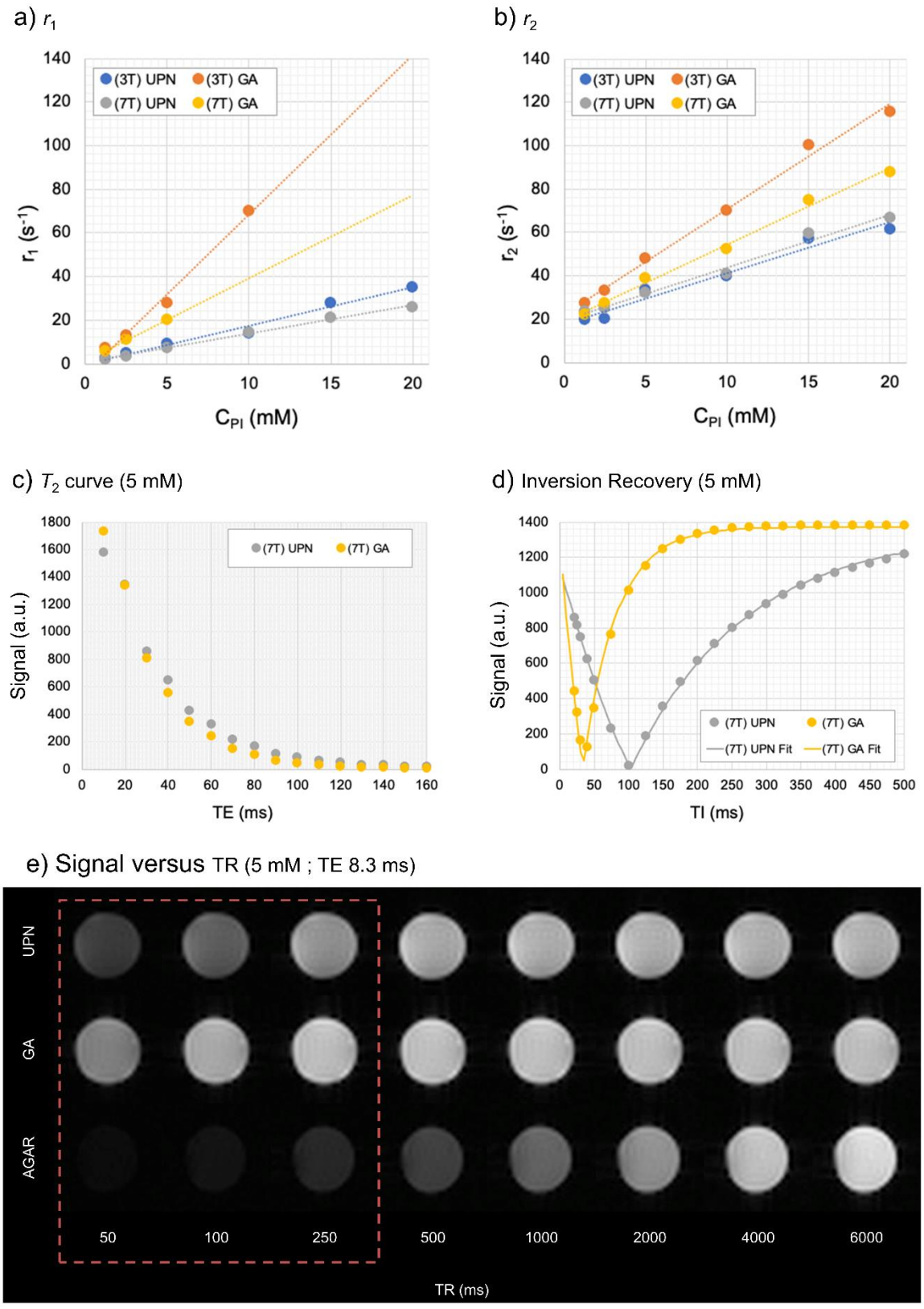

Figure 2. MR relaxometry of UPNs and GA. Comparison of (a) r_1 and (b) r_2 curves obtained at 3T and 7T magnetic fields in agar phantoms with increasing concentrations of the paramagnetic ions. (c) T_2 and (d) Inversion Recovery curves at 5 mM of paramagnetic ion and 7T magnetic field showing the shortening of T_2 and T_1, respectively. (e) Spin Echo images for UPN and GA in agar as compared to

agar control acquired in different TR times emphasizing the hypersignal at low TRs (red square). C_{PI}: concentration of paramagnetic ion (mM).

Furthermore, the T_2 and inversion recovery curves determined for 5 mM of paramagnetic ions in agar at 7T, indicates that UPNs shortens T_2 (**Figure 2c**) and T_1 as well (**Figure 2d**) but less effectively than GA. This is expected considering that Gd^{3+} ($7e^-$) has a larger number of unpaired electrons than Fe^{3+} ($5e^-$), but the difference persists even after normalization using such parameter. The effectiveness of T_1 shortening can be seen in **Figure 2e**, where low TR times results in hypersignal in spin echo sequence when compared with control, showing that the new UPNs also are T_1-CAs.

The UPNs presented a much lower r_2/r_1 ratios at 3 and 7T (1.38 and 1.78) than SPIONs reported in the literature (**Table 1**), clearly evidencing the success of our strategy and nanostructure design based on iron oxide decorated usTiO_2NPs. Ferumoxytol has r_2/r_1 ratio 4.5 times larger than UPNs, while Feridex exhibits an even larger value (r_2/r_1 = 22.7). In short, the controlled deposition of iron oxide on usTiO_2NPs can generate CAs with T_1 and T_2 relaxation characteristics similar to GBCAs. The presence of iron oxide only at the surface of usTiO_2NPs maximizes the number of paramagnetic sites that can interact directly with water molecules in the medium promoting spin relaxation by the spin-lattice mechanism, while minimizing the spin-spin relaxation.

Table 1. Relaxivities of commercial MRI contrast media based on superparamagnetic iron oxide nanoparticles (SPIONs) in comparison with UPN and gadoteric acid (mM^{-1} s^{-1}).

Contrast Agent	r_1	r_2	r_2/r_1	Magnetic field	Reference
Supravist (SHU 555C)	7.3	57	7.8	3T	[48]
Feridex/Endorem	4.1	93	22.7	3T	[48]
Resovist (SHU 555A)	4.6	143	31.1	3T	[48]
Ferumoxytol	10 [a]	62.3 [a]	6.2	3T	[49]
Sinerem	6.58 [b]	127.8 [b]	19.4	3T	[50]
UPN	1.76	2.43	1.38	3T	this work
Gadoteric Acid (GA)	7.32	4.84	0.66	3T	this work
UPN	1.32	2.35	1.78	7T	this work
Gadoteric Acid (GA)	3.80	3.53	0.93	7T	this work

[a] Measured in saline solution

[b] Measured in Ficoll solution

After careful evaluation of the stability of UPNs in biological media, *in vitro* cytotoxicity and efficacy, the potential of the novel UPNs as T_1-contrast agent was further evaluated *in vivo* using Wistar rats (4 males, 2 GA and 2 UPNs) as animal models, using a 7T MR scanner. The images were acquired before and after 20 seconds i.v. bolus injection of GA (0.1 mmol/kg of body weight, 25 mM of GA), or UPN (0.1 mmol/kg of body weight, 25 mM Fe) following a protocol approved by the FMUSP Animal Ethics Committee (#966/2018). The time dependent T_1-weighted MR images (**Figure 3, Movies S1 and S2**) obtained post-injection of the CAs show the enhancement of the brightness in the heart, liver, blood vessels and kidneys (yellow arrows), in comparison to the images obtained before the injection, as expected. In addition, a dynamic study was also performed. Sequences of MR images were obtained along 5 minutes after i.v. injection through penile vein, with temporal resolution of 1.6 seconds. The average signal for 2 animals per group was plotted as a function of time generating time-signal intensity curves (TIC), whose regions of interest (ROI) were manually segmented as shown in the insets. The baseline was corrected considering the signal before the injection of the CAs. The raw signal *vs* time plots (**Figure 4)** suggest the similarity of GA and UPN responses in enhancing the T_1-signal intensity in heart and kidneys soon after the injection of the CAs, in agreement with the MR images shown in **Figure 3**. In the case of heart, the signal increases until peaking and then decreases, as expected for the dilution induced by the heartbeat, indicating that both CAs present similar TIC pattens in heart and kidneys.

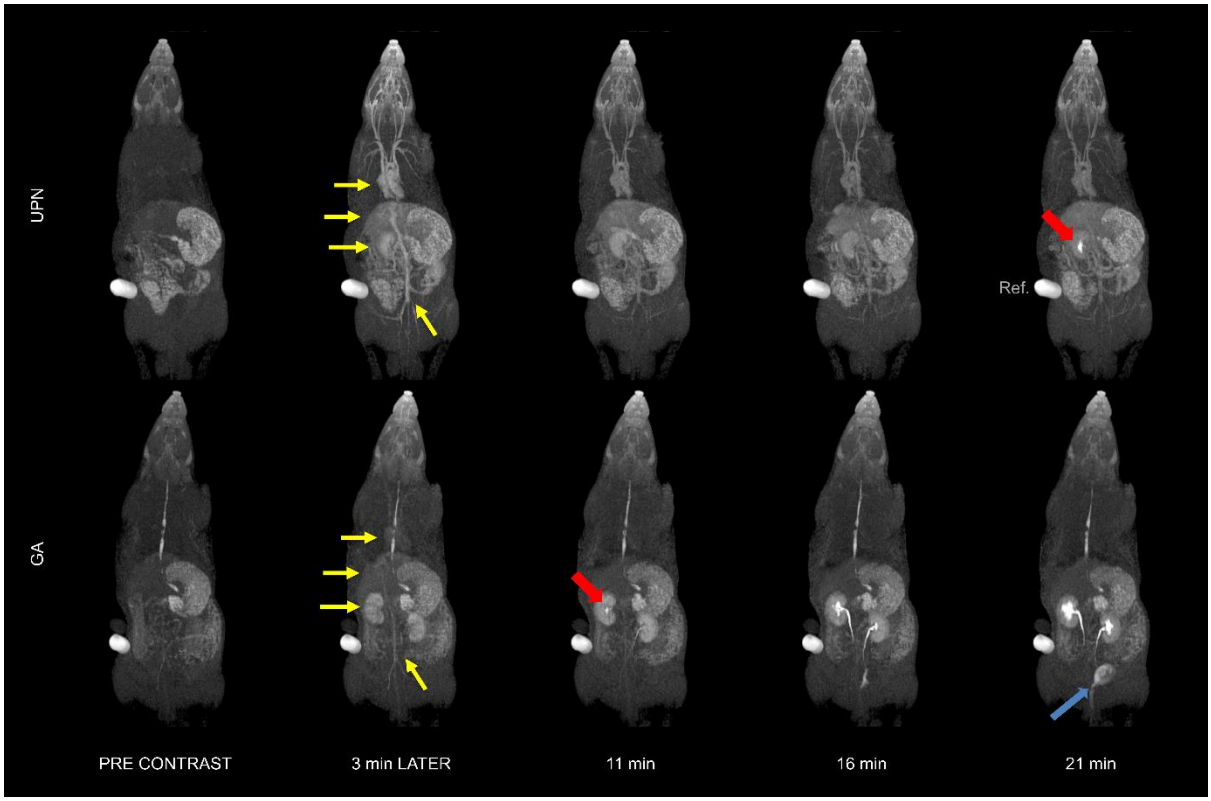

Figure 3. T_1-weighted MR images of Wistar rats before (pre contrast) and 3 min, 11 min, 16 min and 21 min after i.v. bolus injection of (top line) UPN and GA (bottom line) contrast agent. Yellow arrows indicate regions of contrast enhancement after injection of contrast agents: heart, liver, kidneys, and blood vessels. Red arrows show the arrival and accumulation of the contrast agent on the renal calyx at different times. Blue arrow indicates the region of bladder. Ref.: phantom reference prepared by dissolving UPNs in agar.

A more detailed analysis of the time series of T_1-weighted MR images obtained before and after bolus injection of GA and UPN contrast agents shown in **Figure 3** indicates the progressive accumulation of GA in the renal pelvis after 11 min of injection (red arrow), as expected for its preferential elimination by urinary excretion pathway.[51] There is a sharp signal increase at renal pelvis followed by a late and slower intensity enhancement at renal calyx (**Figures 3 and 4**) probably reflecting their molecular and nanoparticulate nature, respectively, on the filtration process by nephrons. Accordingly, the UPN also showed a tendency of renal accumulation and excretion but took a much longer time (21 min) after the injection to start appearing in the kidneys (red arrow in **Figure 3**) and finally in the bladder (blue arrow in **Figure 3**). MR images obtained at longer times suggest the brightness of blood vessels progressively decreases, whilst the brightness of bladder was enhanced (**Figure S2**). The glomerular filtration barrier has a cutoff size of 5-6 nm, thus smaller particles are expected to be filtered from the blood into the kidneys,[52] and been eliminated by urinary

excretion. Therefore, its late accumulation in the renal pelvis may be attributed to the negative surface charge and possible electrostatic repulsion when reaching the glomerular filtration membrane (GFM).[52] Another possibility is due to the biomolecular corona effect, which can increase the hydrodynamic size of UPNs consequently slowing down the crossing rate through the GFM.[52,53] On the other hand, this result also suggests that UPN may have a longer circulation time than GA. This is interesting since it could be used as a blood-pool contrast agent for MR angiography, a technique in which the vasculature structures are imaged.[54–56] In fact it is possible to clearly see the blood vessels of the rat even after more than ten minutes of acquisition of MR images, as shown in **Figure 3**. A more biocompatible material[57] could reduce the nephrotoxicity in patients with renal deficiency while avoiding systemic nephrogenic fibrosis since titanium and iron do not undergo transmetallation *in vivo* in contrast with Gd^{3+}.[58]

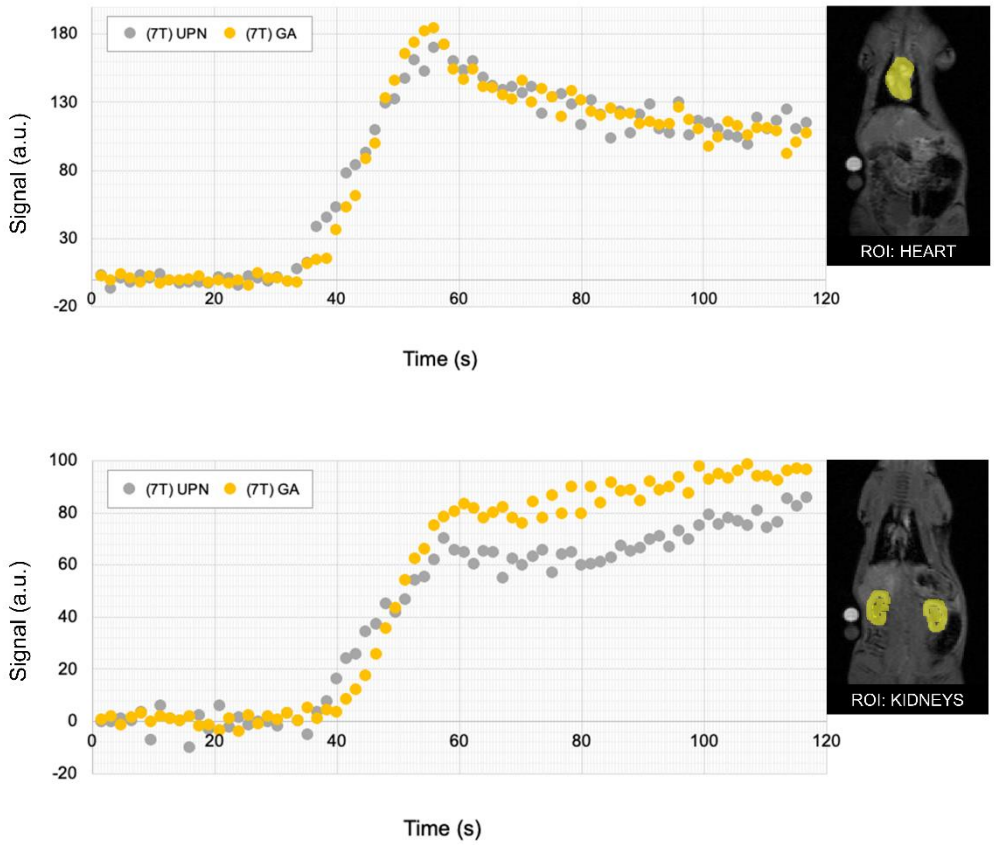

Figure 4. Average of T_1-signal intensity of 2 rats as a function of time in the (top) heart and (bottom) kidneys, as indicated by the respective ROIs, 20-second after i.v. bolus injection of GA and UPN.

Summarizing, the novel ultrasmall paramagnetic nanoparticle designed as T_1-weighted MR contrast agent is fully compatible with the conventional clinical administration protocol and presented relaxometric parameters comparable to the gadoteric acid in agar

phantoms, as well as similar image quality after i.v. bolus injection in Wistar rats. The renal elimination rate of UPN was about half of GA, assuring an exceptional contrast effect for twice as longer time, which can be quite advantageous as blood-pool contrast agent for MR angiography. Furthermore, the UPN exhibited low cytotoxicity against vascular endothelial cells and macrophages used as model cell lines, and a good colloidal stability in biological medium. Those combined features indicate UPN has great potential as alternative to GBCAs in MR imaging and angiography, especially for patients with severe renal impairment, using a similar clinical application protocol.

AUTHOR INFORMATION

Corresponding Author

Koiti Araki - Laboratory of Supramolecular Chemistry and Nanotechnology, Department of Fundamental Chemistry, Institute of Chemistry, Av. Prof. Lineu Prestes, 748, 05508-000, University of Sao Paulo, Sao Paulo, Brazil. Tel: +55 11 3091-8513; orcid.org/0000-0003-3485-4592.

E-mail: koiaraki@iq.usp.br

Rodrigo Ken Kawassaki – Laboratory of Supramolecular Chemistry and Nanotechnology, Department of Fundamental Chemistry, Institute of Chemistry, University of São Paulo, São Paulo 05508-000, Brazil; orcid.org/0000-0002-6497-5072

Mariana Romano – Laboratory of Supramolecular Chemistry and Nanotechnology, Department of Fundamental Chemistry, Institute of Chemistry, University of São Paulo, São Paulo 05508-000, Brazil; orcid.org/0000-0003-2881-2708

Mayara Klimuk Uchiyama – Laboratory of Supramolecular Chemistry and Nanotechnology, Department of Fundamental Chemistry, Institute of Chemistry, University of São Paulo, São Paulo 05508-000, Brazil; Laboratory of Magnetic Resonance in Neuroradiology (LIM44), School of Medicine, University of São Paulo, Av. Dr. Arnaldo, 455, Sao Paulo, 01246-903, Brazil; orcid.org/0000-0002-6623-9765

Maurício da Silva Baptista– Laboratory of Interfaces and Photoinduced Processes, Department of Biochemistry, Institute of Chemistry, University of São Paulo, São Paulo, Brazil; orcid.org/0000-0001-7079-7666

Sandra Helena Poliselli Farsky – Laboratory of Inflammation and Immunotoxicology Department of Clinical and Toxicological Analysis, Faculty of Pharmaceutical Sciences, University of São Paulo, São Paulo, Brazil; orcid.org/0000-0002-3943-977X

Khallil Taverna Chaim – Laboratory of Magnetic Resonance in Neuroradiology (LIM44) and Imaging Platform (PISA), School of Medicine, University of São Paulo, Av. Dr. Arnaldo, 455, Sao Paulo, 01246-903, Brazil; orcid.org/0000-0002-5803-0099

Robson R. Guimarães – Laboratory of Supramolecular Chemistry and Nanotechnology, Department of Fundamental Chemistry, Institute of Chemistry, University of São Paulo, São Paulo 05508-000, Brazil; orcid.org/0000-0002-9825-6690

Notes

The authors declare no competing financial interest.

ACKNOWLEDGMENTS

The authors would like to thank the financial support granted by São Paulo Research Foundation (FAPESP, grants #2019/02151-2 to RKK, #2018/21489-1 to KA and #2009/54323-0 to PISA), National Council for Scientific and Technological Development (CNPq, KA grants 442599/2019-6, 401581/2016-0, 303137/2016-9 and 402281/2013-6), Coordenação de Aperfeiçoamento de Pessoal de Nível Superior (CAPES program 33002010191PO), and to SisNANO-USP. Special acknowledgement to Dr. Helton Nogueira Pereira and Dr. Jefferson Bettini of National Laboratory of Nanotechnology (LNNano/CNPEM) for the TEM image.

REFERENCES

(1) Jeon, M.; Halbert, M. v.; Stephen, Z. R.; Zhang, M. Iron Oxide Nanoparticles as T1 Contrast Agents for Magnetic Resonance Imaging: Fundamentals, Challenges, Applications, and Prospectives. *Adv Mater* **2021**, *33* (23), 1906539. https://doi.org/10.1002/adma.201906539.

(2) Peng, Y.-K.; Tsang, S. C. E.; Chou, P.-T. T. Chemical Design of Nanoprobes for T1-Weighted Magnetic Resonance Imaging. *Mater Today* **2016**, *19* (6), 336–348. https://doi.org/10.1016/j.mattod.2015.11.006.

(3) Lohrke, J.; Frenzel, T.; Endrikat, J.; Alves, F. C.; Grist, T. M.; Law, M.; Lee, J. M.; Leiner, T.; Li, K.-C.; Nikolaou, K.; Prince, M. R.; Schild, H. H.; Weinreb, J. C.;

Yoshikawa, K.; Pietsch, H. 25 Years of Contrast-Enhanced MRI: Developments, Current Challenges and Future Perspectives. *Adv Ther* **2016**, *33*, 1–28. https://doi.org/10.1007/s12325-015-0275-4.

(4) Sudarshana, D. M.; Nair, G.; Dwyer, J. T.; Dewey, B.; Steele, S. U.; Suto, D. J.; Wu, T.; Berkowitz, B. A.; Koretsky, A. P.; Cortese, I. C. M.; Reich, D. S. Manganese-Enhanced MRI of the Brain in Healthy Volunteers. *AJNR Am J Neuroradiol* **2019**, *40* (8), 1309–1316. https://doi.org/10.3174/ajnr.a6152.

(5) Kawassaki, R. K.; Romano, M.; Dietrich, N.; Araki, K. Titanium and Iron Oxide Nanoparticles for Cancer Therapy: Surface Chemistry and Biological Implications. *Front Nanotechnol* **2021**, *3*, 735434. https://doi.org/10.3389/fnano.2021.735434.

(6) Ramalho, J.; Semelka, R. C.; Ramalho, M.; Nunes, R. H.; AlObaidy, M.; Castillo, M. Gadolinium-Based Contrast Agent Accumulation and Toxicity: An Update. *AJNR Am J Neuroradiol* **2016**, *37* (7), 1192–1198. https://doi.org/10.3174/ajnr.A4615.

(7) Rogosnitzky, M.; Branch, S. Gadolinium-Based Contrast Agent Toxicity: A Review of Known and Proposed Mechanisms. *BioMetals* **2016**, *29* (3), 365–376. https://doi.org/10.1007/s10534-016-9931-7.

(8) Layne, K. A.; Dargan, P. I.; Archer, J. R. H.; Wood, D. M. Gadolinium Deposition and the Potential for Toxicological Sequelae - A Literature Review of Issues Surrounding Gadolinium-Based Contrast Agents. *Br J Clin Pharmacol* **2018**, *84* (11), 2522–2534. https://doi.org/10.1111/bcp.13718.

(9) McDonald, R. J.; McDonald, J. S.; Kallmes, D. F.; Jentoft, M. E.; Paolini, M. A.; Murray, D. L.; Williamson, E. E.; Eckel, L. J. Gadolinium Deposition in Human Brain Tissues after Contrast-Enhanced MR Imaging in Adult Patients without Intracranial Abnormalities. *Radiology* **2017**, *285* (2), 546–554. https://doi.org/10.1148/radiol.2017161595.

(10) Caspani, S.; Magalhães, R.; Araújo, J. P.; Sousa, C. T. Magnetic Nanomaterials as Contrast Agents for MRI. *Materials* **2020**, *13* (11), 2586. https://doi.org/10.3390/ma13112586.

(11) Soufi, G. J.; Hekmatnia, A.; Iravani, S.; Varma, R. S. Nanoscale Contrast Agents for Magnetic Resonance Imaging: A Review. *ACS Appl Nano Mater* **2022**, *5* (8), 10151–10166. https://doi.org/10.1021/acsanm.2c03297.

(12) Dadfar, S. M.; Roemhild, K.; Drude, N. I.; von Stillfried, S.; Knüchel, R.; Kiessling, F.; Lammers, T. Iron Oxide Nanoparticles: Diagnostic, Therapeutic and Theranostic

Applications. *Adv Drug Deliv Rev* **2019**, *138*, 302–325. https://doi.org/10.1016/j.addr.2019.01.005.

(13) Park, J. Y.; Baek, M. J.; Choi, E. S.; Woo, S.; Kim, J. H.; Kim, T. J.; Jung, J. C.; Chae, K. S.; Chang, Y.; Lee, G. H. Paramagnetic Ultrasmall Gadolinium Oxide Nanoparticles as Advanced T 1 MRI Contrast Agent: Account for Large Longitudinal Relaxivity, Optimal Particle Diameter, and In Vivo T1 MR Images. *ACS Nano* **2009**, *3* (11), 3663–3669. https://doi.org/10.1021/nn900761s.

(14) Kim, T.; Momin, E.; Choi, J.; Yuan, K.; Zaidi, H.; Kim, J.; Park, M.; Lee, N.; McMahon, M. T.; Quinones-Hinojosa, A.; Bulte, J. W. M.; Hyeon, T.; Gilad, A. A. Mesoporous Silica-Coated Hollow Manganese Oxide Nanoparticles as Positive T 1 Contrast Agents for Labeling and MRI Tracking of Adipose-Derived Mesenchymal Stem Cells. *J Am Chem Soc* **2011**, *133* (9), 2955–2961. https://doi.org/10.1021/ja1084095.

(15) Cao, Y.; Xu, L.; Kuang, Y.; Xiong, D.; Pei, R. Gadolinium-Based Nanoscale MRI Contrast Agents for Tumor Imaging. *J Mater Chem B* **2017**, *5* (19), 3431–3461. https://doi.org/10.1039/c7tb00382j.

(16) Miao, Y.; Xie, Q.; Zhang, H.; Cai, J.; Liu, X.; Jiao, J.; Hu, S.; Ghosal, A.; Yang, Y.; Fan, H. Composition-Tunable Ultrasmall Manganese Ferrite Nanoparticles: Insights into Their *In Vivo* T_1 Contrast Efficacy. *Theranostics* **2019**, *9* (6), 1764–1776. https://doi.org/10.7150/thno.31233.

(17) Cai, Y.; Wang, Y.; Zhang, T.; Pan, Y. Gadolinium-Labeled Ferritin Nanoparticles as T1 Contrast Agents for Magnetic Resonance Imaging of Tumors. *ACS Appl Nano Mater* **2020**, *3* (9), 8771–8783. https://doi.org/10.1021/acsanm.0c01563.

(18) Zheng, X. Y.; Pellico, J.; Khrapitchev, A. A.; Sibson, N. R.; Davis, J. J. Dy-DOTA Integrated Mesoporous Silica Nanoparticles as Promising Ultrahigh Field Magnetic Resonance Imaging Contrast Agents. *Nanoscale* **2018**, *10* (45), 21041–21045. https://doi.org/10.1039/c8nr07198e.

(19) Marasini, R.; Rayamajhi, S.; Moreno-Sanchez, A.; Aryal, S. Iron(III) Chelated Paramagnetic Polymeric Nanoparticle Formulation as a next-Generation T1-Weighted MRI Contrast Agent. *RSC Adv* **2021**, *11* (51), 32216–32226. https://doi.org/10.1039/d1ra05544e.

(20) Jin, R.; Lin, B.; Li, D.; Ai, H. Superparamagnetic Iron Oxide Nanoparticles for MR Imaging and Therapy: Design Considerations and Clinical Applications. *Curr Opin Pharmacol* **2014**, *18*, 18–27. https://doi.org/10.1016/j.coph.2014.08.002.

(21) Feng, Q.; Liu, Y.; Huang, J.; Chen, K.; Huang, J.; Xiao, K. Uptake, Distribution, Clearance, and Toxicity of Iron Oxide Nanoparticles with Different Sizes and Coatings. *Sci Rep* **2018**, *8*, 2082. https://doi.org/10.1038/s41598-018-19628-z.

(22) Sangnier, A. P.; Walle, A. B. van de; Curcio, A.; Borgne, R. le; Motte, L.; Lalatonne, Y.; Wilhelm, C. Impact of Magnetic Nanoparticle Surface Coating on Their Long-Term Intracellular Biodegradation in Stem Cells. *Nanoscale* **2019**, *11*, 16488–16498. https://doi.org/10.1039/c9nr05624f.

(23) Na, H. bin; Song, I. C.; Hyeon, T. Inorganic Nanoparticles for MRI Contrast Agents. *Adv Mater* **2009**, *21* (21), 2133–2148. https://doi.org/10.1002/adma.200802366.

(24) Nosrati, H.; Salehiabar, M.; Fridoni, M.; Abdollahifar, M.-A.; Manjili, H. K.; Davaran, S.; Danafar, H. New Insight about Biocompatibility and Biodegradability of Iron Oxide Magnetic Nanoparticles: Stereological and In Vivo MRI Monitor. *Sci Rep* **2019**, *9*, 7173. https://doi.org/10.1038/s41598-019-43650-4.

(25) Tromsdorf, U. I.; Bruns, O. T.; Salmen, S. C.; Beisiegel, U.; Weller, H. A Highly Effective, Nontoxic T1 MR Contrast Agent Based on Ultrasmall PEGylated Iron Oxide Nanoparticles. *Nano Lett* **2009**, *9* (12), 4434–4440. https://doi.org/10.1021/nl902715v.

(26) Kim, B. H.; Lee, N.; Kim, H.; An, K.; Park, Y. il; Choi, Y.; Shin, K.; Lee, Y.; Kwon, S. G.; Na, H. bin; Park, J.-G.; Ahn, T.-Y.; Kim, Y.-W.; Moon, W. K.; Choi, S. H.; Hyeon, T. Large-Scale Synthesis of Uniform and Extremely Small-Sized Iron Oxide Nanoparticles for High-Resolution T 1 Magnetic Resonance Imaging Contrast Agents. *J Am Chem Soc* **2011**, *133* (32), 12624–12631. https://doi.org/10.1021/ja203340u.

(27) Shen, Z.; Chen, T.; Ma, X.; Ren, W.; Zhou, Z.; Zhu, G.; Zhang, A.; Liu, Y.; Song, J.; Li, Z.; Ruan, H.; Fan, W.; Lin, L.; Munasinghe, J.; Chen, X.; Wu, A. Multifunctional Theranostic Nanoparticles Based on Exceedingly Small Magnetic Iron Oxide Nanoparticles for T1-Weighted Magnetic Resonance Imaging and Chemotherapy. *ACS Nano* **2017**, *11* (11), 10992–11004. https://doi.org/10.1021/acsnano.7b04924.

(28) Wei, H.; Bruns, O. T.; Kaul, M. G.; Hansen, E. C.; Barch, M.; Wiśniowska, A.; Chen, O.; Chen, Y.; Li, N.; Okada, S.; Cordero, J. M.; Heine, M.; Farrar, C. T.; Montana, D. M.; Adam, G.; Ittrich, H.; Jasanoff, A.; Nielsen, P.; Bawendi, M. G. Exceedingly Small Iron Oxide Nanoparticles as Positive MRI Contrast Agents. *Proc Natl Acad Sci U S A* **2017**, *114* (9), 2325–2330. https://doi.org/10.1073/pnas.1620145114.

(29) Ma, D.; Chen, J.; Luo, Y.; Wang, H.; Shi, X. Zwitterion-Coated Ultrasmall Iron Oxide Nanoparticles for Enhanced T1-Weighted Magnetic Resonance Imaging Applications. *J Mater Chem B* **2017**, *5*, 7267–7273. https://doi.org/10.1039/c7tb01588g.

(30) Bao, Y.; Sherwood, J. A.; Sun, Z. Magnetic Iron Oxide Nanoparticles as T1 Contrast Agents for Magnetic Resonance Imaging. *J Mater Chem C Mater* **2018**, *6*, 1280–1290. https://doi.org/10.1039/c7tc05854c.

(31) Li, F.; Liang, Z.; Liu, J.; Sun, J.; Hu, X.; Zhao, M.; Liu, J.; Bai, R.; Kim, D.; Sun, X.; Hyeon, T.; Ling, D. Dynamically Reversible Iron Oxide Nanoparticle Assemblies for Targeted Amplification of T1-Weighted Magnetic Resonance Imaging of Tumors. *Nano Lett* **2019**, *19* (7), 4213–4220. https://doi.org/10.1021/acs.nanolett.8b04411.

(32) Nguyen, K. L.; Yoshida, T.; Kathuria-Prakash, N.; Zaki, I. H.; Varallyay, C. G.; Semple, S. I.; Saouaf, R.; Rigsby, C. K.; Stoumpos, S.; Whitehead, K. K.; Griffin, L. M.; Saloner, D.; Hope, M. D.; Prince, M. R.; Fogel, M. A.; Schiebler, M. L.; Roditi, G. H.; Radjenovic, A.; Newby, D. E.; Neuwelt, E. A.; Bashir, M. R.; Hu, P.; Paul Finn, J. Multicenter Safety and Practice for Off-Label Diagnostic Use of Ferumoxytol in MRI. *Radiology* **2019**, *293* (3), 554–564. https://doi.org/10.1148/radiol.2019190477.

(33) Toma, S. H.; Santos, J. J.; da Silva, D. G.; Huila, M. F. G.; Toma, H. E.; Araki, K. Improving Stability of Iron Oxide Nanofluids for Enhanced Oil Recovery: Exploiting Wettability Modifications in Carbonaceous Rocks. *J Pet Sci Eng* **2022**, *212*, 110311. https://doi.org/10.1016/j.petrol.2022.110311.

(34) Moore, T. L.; Rodriguez-Lorenzo, L.; Hirsch, V.; Balog, S.; Urban, D.; Jud, C.; Rothen-Rutishauser, B.; Lattuada, M.; Petri-Fink, A. Nanoparticle Colloidal Stability in Cell Culture Media and Impact on Cellular Interactions. *Chem Soc Rev* **2015**, *44* (17), 6287–6305. https://doi.org/10.1039/c4cs00487f.

(35) Zook, J. M.; MacCuspie, R. I.; Locascio, L. E.; Halter, M. D.; Elliott, J. T. Stable Nanoparticle Aggregates/Agglomerates of Different Sizes and the Effect of Their Size on Hemolytic Cytotoxicity. *Nanotoxicology* **2011**, *5* (4), 517–530. https://doi.org/10.3109/17435390.2010.536615.

(36) Albanese, A.; Chan, W. C. W. Effect of Gold Nanoparticle Aggregation on Cell Uptake and Toxicity. *ACS Nano* **2011**, *5* (7), 5478–5489. https://doi.org/10.1021/nn2007496.

(37) Lankoff, A.; Sandberg, W. J.; Wegierek-Ciuk, A.; Lisowska, H.; Refsnes, M.; Sartowska, B.; Schwarze, P. E.; Meczynska-Wielgosz, S.; Wojewodzka, M.; Kruszewski, M. The Effect of Agglomeration State of Silver and Titanium Dioxide

Nanoparticles on Cellular Response of HepG2, A549 and THP-1 Cells. *Toxicol Lett* **2012**, *208* (3), 197–213. https://doi.org/10.1016/j.toxlet.2011.11.006.

(38) Alkilany, A. M.; Mahmoud, N. N.; Hashemi, F.; Hajipour, M. J.; Farvadi, F.; Mahmoudi, M. Misinterpretation in Nanotoxicology: A Personal Perspective. *Chem Res Toxicol* **2016**, *29* (6), 943–948. https://doi.org/10.1021/acs.chemrestox.6b00108.

(39) Ta, H. T.; Li, Z.; Wu, Y.; Cowin, G.; Zhang, S.; Yago, A.; Whittaker, A. K.; Xu, Z. P. Effects of Magnetic Field Strength and Particle Aggregation on Relaxivity of Ultra-Small Dual Contrast Iron Oxide Nanoparticles. *Mater Res Express* **2017**, *4* (116105), 116105. https://doi.org/10.1088/2053-1591/aa96e3.

(40) Wang, L.; Huang, J.; Chen, H.; Wu, H.; Xu, Y.; Li, Y.; Yi, H.; Wang, Y. A.; Yang, L.; Mao, H. Exerting Enhanced Permeability and Retention Effect Driven Delivery by Ultrafine Iron Oxide Nanoparticles with T1-T2 Switchable Magnetic Resonance Imaging Contrast. *ACS Nano* **2017**, *11* (5), 4582–4592. https://doi.org/10.1021/acsnano.7b00038.

(41) Tsoi, K. M.; MacParland, S. A.; Ma, X.-Z.; Spetzler, V. N.; Echeverri, J.; Ouyang, B.; Fadel, S. M.; Sykes, E. A.; Goldaracena, N.; Kaths, J. M.; Conneely, J. B.; Alman, B. A.; Selzner, M.; Ostrowski, M. A.; Adeyi, O. A.; Zilman, A.; McGilvray, I. D.; Chan, W. C. W. Mechanism of Hard-Nanomaterial Clearance by the Liver. *Nat Mater* **2016**, *15* (11), 1212–1221. https://doi.org/10.1038/nmat4718.

(42) Poon, W.; Zhang, Y. N.; Ouyang, B.; Kingston, B. R.; Wu, J. L. Y.; Wilhelm, S.; Chan, W. C. W. Elimination Pathways of Nanoparticles. *ACS Nano* **2019**, *13* (5), 5785–5798. https://doi.org/10.1021/acsnano.9b01383.

(43) Ferretti, A. M.; Usseglio, S.; Mondini, S.; Drago, C.; la Mattina, R.; Chini, B.; Verderio, C.; Leonzino, M.; Cagnoli, C.; Joshi, P.; Boraschi, D.; Italiani, P.; Li, Y.; Swartzwelter, B. J.; Sironi, L.; Gelosa, P.; Castiglioni, L.; Guerrini, U.; Ponti, A. Towards Bio-Compatible Magnetic Nanoparticles: Immune-Related Effects, in-Vitro Internalization, and in-Vivo Bio-Distribution of Zwitterionic Ferrite Nanoparticles with Unexpected Renal Clearance. *J Colloid Interface Sci* **2021**, *582* (B), 678–700. https://doi.org/10.1016/j.jcis.2020.08.026.

(44) International Organization for Standardization. *ISO 10993-5:2009 - Biological Evaluation of Medical Devices — Part 5: Tests for in Vitro Cytotoxicity*. Geneva, Switzerland **2009**. https://www.iso.org/standard/36406.html (accessed 2022-01-27).

(45) Pozzi, D.; Caracciolo, G.; Digiacomo, L.; Colapicchioni, V.; Palchetti, S.; Capriotti, A. L.; Cavaliere, C.; Zenezini Chiozzi, R.; Puglisi, A.; Laganà, A. The Biomolecular

514 Corona of Nanoparticles in Circulating Biological Media. *Nanoscale* **2015**, *7* (33),
515 13958–13966. https://doi.org/10.1039/c5nr03701h.
516 (46) Merz, V.; Lenhart, J.; Vonhausen, Y.; Ortiz-Soto, M. E.; Seibel, J.; Krueger, A.
517 Zwitterion-Functionalized Detonation Nanodiamond with Superior Protein Repulsion
518 and Colloidal Stability in Physiological Media. *Small* **2019**, *15* (48), 1901551.
519 https://doi.org/10.1002/smll.201901551.
520 (47) Hadjidemetriou, M.; Kostarelos, K. Nanomedicine: Evolution of the Nanoparticle
521 Corona. *Nat Nanotechnol* **2017**, *12*, 288–290. https://doi.org/10.1038/nnano.2017.61.
522 (48) Rohrer, M.; Bauer, H.; Mintorovitch, J.; Requardt, M.; Weinmann, H.-J. Comparison
523 of Magnetic Properties of MRI Contrast Media Solutions at Different Magnetic Field
524 Strengths. *Invest Radiol* **2005**, *40* (11), 715–724.
525 https://doi.org/10.1097/01.rli.0000184756.66360.d3.
526 (49) Knobloch, G.; Colgan, T.; Wiens, C. N.; Wang, X.; Schubert, T.; Hernando, D.;
527 Sharma, S. D.; Reeder, S. B. Relaxivity of Ferumoxytol at 1.5 T and 3.0 T. *Invest*
528 *Radiol* **2018**, *53* (5), 257–263. https://doi.org/10.1097/rli.0000000000000434.
529 (50) Simon, G. H.; Bauer, J.; Saborovski, O.; Fu, Y.; Corot, C.; Wendland, M. F.; Daldrup-
530 Link, H. E. T1 and T2 Relaxivity of Intracellular and Extracellular USPIO at 1.5T and
531 3T Clinical MR Scanning. *Eur Radiol* **2006**, *16* (3), 738–745.
532 https://doi.org/10.1007/S00330-005-0031-2.
533 (51) Tartaro, A.; Maccarone, M. T. The Utility of Gadoteric Acid in Contrast-Enhanced
534 MRI: A Review. *Rep Med Imaging* **2015**, *8*, 25–35.
535 https://doi.org/10.2147/rmi.s46798.
536 (52) Du, B.; Yu, M.; Zheng, J. Transport and Interactions of Nanoparticles in the Kidneys.
537 *Nat Rev Mater* **2018**, *3* (10), 358–374. https://doi.org/10.1038/s41578-018-0038-3.
538 (53) Adhipandito, C. F.; Cheung, S. H.; Lin, Y. H.; Wu, S. H. Atypical Renal Clearance of
539 Nanoparticles Larger Than the Kidney Filtration Threshold. *Int J Mol Sci* **2021**, *22*
540 (20), 11182. https://doi.org/10.3390/ijms222011182.
541 (54) Park, E.-A.; Lee, W.; So, Y. H.; Lee, Y.-S.; Jeon, B.-S.; Choi, K. S.; Kim, E.-G.;
542 Myeong, W.-J. Extremely Small Pseudoparamagnetic Iron Oxide Nanoparticle as a
543 Novel Blood Pool T1 Magnetic Resonance Contrast Agent for 3 T Whole-Heart
544 Coronary Angiography in Canines: Comparison With Gadoterate Meglumine. *Invest*
545 *Radiol* **2017**, *52* (2), 128–133. https://doi.org/10.1097/rli.0000000000000321.
546 (55) Vangijzegem, T.; Stanicki, D.; Boutry, S.; Paternoster, Q.; vander Elst, L.; Muller, R.
547 N.; Laurent, S. VSION as High Field MRI T1 Contrast Agent: Evidence of Their

548 Potential as Positive Contrast Agent for Magnetic Resonance Angiography.
549 *Nanotechnology* **2018**, *29* (26), 265103. https://doi.org/10.1088/1361-6528/aabbd0.
550 (56) Wagner, M.; Wagner, S.; Schnorr, J.; Schellenberger, E.; Kivelitz, D.; Krug, L.;
551 Dewey, M.; Laule, M.; Hamm, B.; Taupitz, M. Coronary MR Angiography Using
552 Citrate-Coated Very Small Superparamagnetic Iron Oxide Particles as Blood-Pool
553 Contrast Agent: Initial Experience in Humans. *J Magn Reson Imaging* **2011**, *34* (4),
554 816–823. https://doi.org/10.1002/jmri.22683.
555 (57) Weng, Q.; Hu, X.; Zheng, J.; Xia, F.; Wang, N.; Liao, H.; Liu, Y.; Kim, D.; Liu, J.; Li,
556 F.; He, Q.; Yang, B.; Chen, C.; Hyeon, T.; Ling, D. Toxicological Risk Assessments of
557 Iron Oxide Nanocluster- and Gadolinium-Based T1MRI Contrast Agents in Renal
558 Failure Rats. *ACS Nano* **2019**, *13* (6), 6801–6812.
559 https://doi.org/10.1021/acsnano.9b01511.
560 (58) Thakral, C.; Abraham, J. L. Gadolinium-induced nephrogenic systemic fibrosis is
561 associated with insoluble Gd deposits in tissues: in vivo transmetallation confirmed by
562 microanalysis. *J Cutan Pathol* **2009** *36* (12), 1244-54.
563 https://doi.org/10.1111/j.1600-0560.2009.01283.x.
564